UNIVERSIDADE DE SÃO PAULO

INSTITUTO DE FÍSICA
CAIXA POSTAL 20516
01000 - SÃO PAULO - SP
BRASIL

publicações

IFUSP/P-352

YRAST AND HIGH SPIN STATES IN ^{22}Ne

by

E.M. Szanto and A. Szanto de Toledo

Instituto de Física, Universidade de São Paulo,
Lab. Pelletron - C. Postal 20516, São Paulo, Brasil

H.V. Klapdor, G. Rosner and M. Schrader

Max-Planck Institut für Kernphysik, Heidelberg
6900 - Germany

Agosto/1982

YRAST AND HIGH SPIN STATES IN ^{22}Ne

E.M. Szanto and A. Szanto de Toledo
Instituto de Física, Universidade de São Paulo
Lab. Pelletron - C.Postal 20516, São Paulo, Brasil

H.V. Klapdor, G. Rosner and M. Schrader
Max-Planck Institut für Kernphysik, Heidelberg
6900 - Germany

ABSTRACT

High spin states in ^{22}Ne have been investigated by the reactions $^{11}B(^{13}C,d)^{22}Ne$ and $^{13}C(^{11}B,d)^{22}Ne$ up to $E^* \simeq 19MeV$. Yrast states were observed at 11.02 MeV (8^+) and 15.46 MeV (10^+) excitation energy. A backbending in ^{22}Ne is observed around spin 8^+. The location of high spin states $I \leq 10$ is discussed in terms of the rotational band structure, Strutinsky type calculations, and pure shell model predictions.

[Nuclear Reactions $^{11}B(^{13}C,d)^{22}Ne$ and $^{13}C(^{11}B,d)^{22}Ne$ - E_{CM} = 19MeV measured $\sigma(\theta)$, deduced ^{22}Ne high-spin states and compound nucleus ^{24}Na critical angular momentum, Hauser-Feshbach analysis.]

I. INTRODUCTION

In recent years nuclei in the first half of the s-d shell have been subject of considerable interest and effort in the investigation of yrast and high spin states. The extent to which the rotational band structure persists[1] in highly excited deformed light nuclei still remains an open question. On the theoretical side, in particular the extension of the Strutinsky method to rotating nuclei has made it possible to describe the drastic shape-changes often associated with high frequency rotations[2,3].

Among a number of models, the nuclear shell model by means of residual forces can induce strong configuration mixings which can sometimes be interpreted as rotational motion. The excitation spectra of the s-d shell nuclei are sufficiently varied and complex but still not beyond possible description of the complete untruncated s-d basis[4-7]. Therefore phenomena like backbending, etc, can possibly be related to a particular microscopic mechanism in a more unique way than in heavy nuclei. Moreover, in this mass region, in contrast to heavier rare-earth nuclei, a purely microscopic (shell model) description and macroscopic (collective and Strutinsky) methods can be applied to the same phenomena and thus be compared with each other[8,9].

The ^{22}Ne nucleus lying between the two best known light nuclei ^{20}Ne and ^{24}Mg is one of the most highly deformed light nuclei[10,11].

However the confinement of the experimental knowledge of ^{22}Ne to the region $E \lesssim 11$ MeV reflects the extreme experimental difficulties in the observation and identification of the high lying high spin states. This is mainly due to the high level density and the low threshold for particle emission that restricts

the applicability of particle-γ correlation studies to excitation energies of about 10 MeV in ^{22}Ne.

By means of angular correlation measurements, the yrast line of ^{22}Ne is at present clearly identified up to the 6^+ state at 6.305 MeV, a member of the $K^\pi = 0^+$ band build on the ^{22}Ne ground state[12,13]. The 8^+ yrast state has been observed at 11.02 MeV and recently the yrast line has been defined up to the 10^+ state found at 15.46 MeV excitation energy[14]. This last assignment defined a backbending in the ^{22}Ne yrast line around spin 8.

The ^{20}Ne nucleus was the only light nucleus which showed clear experimental evidence for a backbending at a relatively low excitation energy[10]. This effect has been successfully reproduced by shell model calculations using the full s-d shell basis. Arima et al.[4], truncating the shell-model space with the SU(3) group, predicted an irregularity in the yrast line of ^{22}Ne (backbending) around spin 8 and the position of the 10^+ yrast state at 15.8 MeV.

The shell model has been applied in the prediction of rotational bands in ^{22}Ne and very recently the alternative method, the Strutinsky procedure for rotating nuclei has been applied to light nuclei in the mass range A ∿ 20-50. Using a deformed single-particle model this method allows the description of states with higher spins than those accessible in shell model calculations[3]. However due to the fact that residual interactions are very difficult to be considered at the present stage, the Strutinsky method is not directly applicable to the calculation of lower spin states ($I \lesssim 8\hbar$) where pairing interaction play a very important role[15]. Nevertheless it yields very useful qualitative informations on deformations, moments of inertia and shapes of these states, when

compared to the experimental data.

Heavy-Ion Compound Reactions and exploitation of their high spin selectivety have permitted investigation of previously inaccessible high spin states, enlarging the aplicability of particle spectroscopy[11]. Heavy ions carry large amounts of angular momentum into reactions even at relatively low velocities, and can be perfeclty energy-and-angular-momentum matched for high spin spectroscopy of s-d nuclei.

In order to investigate high spin states in ^{22}Ne the ^{11}B(^{13}C,d)^{22}Ne and ^{13}C(^{11}B,d)^{22}Ne reactions have been used to reach highly excited states.

These reactions showed to be the most high spin selective in the 8 MeV < E* < 20 MeV excitation energy interval than the other few possible heavy ion reactions (fig.1). The high channel spins available favours a high statistical fluctuation damping, increasing the accuracy of the Hauser-Feshbach analysis in the interpretation of the experimental results.

Since no γ-decay study has been performed in the present work, information on the ^{22}Ne rotational behaviour can only be inferred through the comparison of the experimental results with the existing theoretical predictions.

II. EXPERIMENTAL PROCEDURE

The $^{11}B(^{13}C,d)^{22}Ne$ and $^{13}C(^{11}B,d)^{22}Ne$ reactions have been studied at the center of mass energy E_{CM} = 19.0 MeV (E_{LAB} = 41.36 MeV and E_{LAB} = 35.0 MeV respectively) using the $^{13}C^{4+}$ and $^{11}B^{4+}$ beams of the MP-Tandem accelerator at Heidelberg.

These two reactions were investigated at the same center of mass energy in order to observe the predominance of compound reaction mechanism, as well as to identify the contribution of contaminants, mainly in the $^{13}C(^{11}B,d)^{22}Ne$ where it was very difficult to eliminate the contribution of ^{12}C contamination (i.e. transitions leading to ^{21}Ne). These transitions were also identified using spectra of the $^{12}C(^{11}B,d)^{21}Ne$ (Q_o = 1.26 MeV) reaction investigated at the same E_{LAB} = 35 MeV energy[16].

Reaction products were detected in 15 gaps of the multigap magnetic spectrograph in the angular range $\theta_{LAB} = 5.5^o$ to $\theta_{LAB} = 90^o$ in steps of 4^o and 7^o. Nuclear track plates of the type Ilford K2 were exposed and scanned (human scanning) in steps of 0,5 mm. A mean solid angle of 3.4×10^{-4} sr was used. A dispersion of ∿13 keV/mm permitted to observe at each 120 cm focal plane an excitation energy interval of ∿15 MeV, and states up to E* ≈ 19 MeV excitation energy have been investigated in the present work.

Typical spectra are shown in fig. 2ab. An overall energy resolution of 60 ∿ 80 keV FWHM (full width at half maximum) was achieved, and was mainly due to the target thickness. Self supporting ^{11}B and ^{13}C (∿25 μg/cm²) targets of isotopically pure (> 96%) material were used. The beam current (1 μA(^{13}C) and 350 nA (^{11}B)) was integrated with an external Faraday cup and exposures of ∿100 mC were used. Possible target deterioration was

monitored by a solid state telescope set at a forward angle to observe the elastically scattered particles.

The excitation energies were determined within an uncertainty of $\Delta E^* \leq 25$ keV for states with E* < 12 MeV and $\Delta E^* \leq 50$ keV for states with 12 MeV < E* < 18 MeV. States denoted with an asterisc in table I were used as reference in the calibration procedure which utilize a second degree polynomial. For unknown levels, a least square fit of the position shift in the focal plane, with respect to the kinematical prediction, was made.

Experimental cross-sections were obtained using a least square peak fitting program JASPER[16] based on symmetrical gaussian peak shapes and by a second order polynomial for background definition in small excitations energy regions. The ambiguity in the definition of the background, mainly in the high excitation energy region is reflected in the uncertainty attributed to the differencial cross-section. The FWHM was assumed to be equal for neighbouring peaks in the spectra. A typical fit is shown in figure 3.

Angular distributions were measured for 82 states. Those obtained by means of the $^{13}C(^{11}B,d)^{22}Ne$ reaction being the inverse reaction of $^{11}B(^{13}C,d)^{22}Ne$ are presented as backward angle in the center of mass frame. However due to the non negligible amount of ^{12}C build-up observed, some transitions to high spin states in ^{21}Ne where not identified clearly and are not reported.

At the bombarding energy used in the present experiment, the grazing angular momentum in the entrance channel obtained by optical model transmission coefficients was ∿14ħ (see fig.1). The energy balance of the reaction allows that states up to ∿20 MeV excitation can be populated. The low orbital angular momentum

carried by the deuterons favours the high spin selectivity of the reaction in the region 8 MeV < E* < 15 MeV, 6ħ < I < 10ħ.

III. THE STATISTICAL MODEL ANALYSIS

The measured angular distributions were analysed within the statistical model. The formalism of the statistical model can be found elsewhere e.g. ref. 17, 18. The angle integrated cross-section averaged over the Ericson fluctuations for the excitation of an individual state with spin I_B at an excitation energy E_B^* in the reaction A(a,b)B is calculated by the relation:

$$\sigma(E_B^*, I_B) = \sum_{J=0}^{J_{max}} \sigma_{CN}(J) G(E_B^*, I_B, J)/g(J) = \sum_{J=0}^{J_{max}} \sigma_J(E_B^*, I_B) \qquad (1)$$

where $\sigma_{CN}(J)$ represents the partial cross section for the formation of a compound nucleus with spin J.

The partial and total decay width of the compound nucleus, $G(E_B^*, I_B^*, J)$ and $g(J)$ respectively, as well as the compound nucleus formation cross sections (σ_{CN}), were calculated using transmission coefficients (T_ℓ) obtained with optical potentials, defined by the parameters listed in table II. The Fermi-gas

expression[19,20] was employed to compute the level density. Calculations of total and differential cross-sections were performed using the code STATIS[21], and all parameters used are listed in table II.

The summation limit J_{max} in equations 1 representing the critical angular momentum for the formation of a compound nucleus has to be determined correctly in order to obtain the right cross sections magnitudes. Partial cross sections σ_J as well as the effect of the truncation at J_{max} on the cross sections is shown in fig.4, for different spin states.

The simultaneous least square fits to all relative differential cross sections $\sigma_{exp}(E^*,I)$, of transitions to states (E^*) of known spin I, as a function of the angular momentum cutoff (J_{max}) in the Hauser-Feshbach expression $\sigma_{H.F.}$ (eq.1) (see ref.11) gives the critical angular momentum in the ^{24}Na compound nucleus at the excitation energy of 39.17 MeV.

The expression:

$$\chi^2_{red} = \frac{1}{N-1}\left[\sum_{\theta,E^*}\left(\frac{\sigma_{exp}(E^*,I) - f(\alpha,a,J_{max})\sigma_{HF}(\theta,E^*,I,\alpha,a,J_{max})}{\varepsilon_{exp}}\right)^2\right]_{min} \qquad (2)$$

was minimized by varying the normalization factor $f(\alpha,a,J_{max})$, in order to use relative experimental cross sections, and remove the dependence of the cross sections on the exact knowledge of the level density parameters, that drastically affect the absolute Hauser-Feshbach cross sections σ_{HF}. In this expression, α denotes any unspecified parameters involved in the computation of σ_{HF}, $\underline{a}$ represents the level density parameters and ε_{exp} is the experimental

uncertainty in cross section.

The value $J_{max} = 13\hbar \pm 1\hbar$ was obtained independently by both reactions using a wide range level density parameter a ($A/10 < a < A/4$)[14]. Since a sharp cutoff approximation is used in the Hauser-Feshbach expression (eq.1), only integer J_{max} values are used, and this is reflected in a variation of the J_{max} value obtained by eq.2 within a range of one unit of $\hbar$, depending on the optical model parameters used (mainly in the exit channel) and on the level density parameters (a,σ). Using an average level density A/6.5 in reference 14 a $J_{max} \approx 12\hbar$ was obtained. The use of average parameters ($a = A/const$) is acceptable when a great number of decay channels are available and taken into account. However, when a few number of channels are considered (six in the present case), and the channel of interest is not the most probable (the present case the α, n and p channels have the highest cross sections respectively), individual level densities parameters are recomended in order not to underweight the channel of interest, and in order to reproduce the partial decay cross sections observed in fusion experiments[22]. In the present work we adopted the parameters listed in table II.

It has been shown[23] that when high spin states are populated (comparable to the critical angular momentum of the compound nucleus) the angular distribution becomes less anisotropic in a way that the shape (anisotropy) of the angular distribution depends of the high spin final state. This effect is clearly shown in fig.5. The reason of this depencence is that the strong alignment of the compound-nucleus spin with the orbital angular momentum of the emitted particle (responsible for the classical $1/\sin\theta$ distribution when low-spin final states are populated) is

lost for final spins comparable to J_{max}.

This shape dependence has been used in the spin determination of states at high excitation energies ($E^* > 10$ MeV), where the level density is higher, and the possibility of a cluster of low spin states simulating a high spin state cannot be ruled out completely by a fit to the absolute angular distribution[11,14]. In the case of a non resolved cluster, the anisotropy of the experimental cross section will be given mainly by the highest spin state of the supposed cluster.

IV. EXPERIMENTAL RESULTS

The results of the analysis of the experimental angular distributions of the $^{11}B(^{13}C,d)^{22}Ne$ and $^{13}C(^{11}B,d)^{22}Ne$ reactions are presented in table I and fig.6a-f. The spin attribution is based on χ^2 fits to the absolute angular distributions by the statistical model calculations. For highly excited states χ^2 fits to the shape of the angular distributions by Hauser-Feshbach calculations, as a function of the spin of the final state have been also performed. Good agreement is obtained between experimental and theoretical angular distributions for states of known spin, the latter taken from references 24-34. A discussion of some individual identified levels follows.

IV.1. THE ^{22}Ne YRAST STATES

In this section we will concentrate only on the ^{22}Ne yrast states that were clearly identified only up to the 6^+ state at 6.305 MeV, a member of the $K^\pi = 0^+$ band, build on the ^{22}Ne ground state. The spin of this state has been measured by means of particle-γ correlation experiments. Broude et al.[12] suggested a candidate for the 8^+ yrast state at 11.00 MeV based on the ^{19}F(α,pγ) experiment. Our present work confirmed this expectation, fitting a 8 spin value to the state observed at 11.05 MeV excitation energy. χ^2 fits both to absolute cross sections as well as to shape of the angular distributions of the yrast states are shown in figure 7a-b. The lowest 10^+ state has been found at 15.46 MeV excitation energy and χ^2 fits for the assignments are within the 97% confidence level. Fits for several possible doublets show, however, that the possibility of one unit lower in $\hbar$ for these yrast states cannot be completely ruled out.

It is known that the statistical fluctuations[17] (Ericson fluctuations) that affect the magnitude of the cross sections could lead to wrong spin assignments when comparing the experimental data to the averaged Hauser-Feshbach cross section. However in our case,due to the high-channel-spin involved, the total effective number of independent open channels for decay of the compound nucleus is high, see fig. 8. Thus the statistical fluctuations are seen to be quite strongly damped already at relatively small angles.

IV.2. HIGH SPIN STATES IN ^{22}Ne

The known level properties of the low-lying states in ^{22}Ne determined through heavy-ion reactions and by particle-γ correlations have been summarized by Endt and Van der Leun[24]. The comparison of our angular distributions with statistical-model calculations (see fig. 6 and table I) shows that the extracted spin values agree with values reported previously. Some additional ^{22}Ne high-spin-states are reported. The experimental level scheme obtained from the present work is depicted in figure 9.

The 3.36 MeV level is known to be the 4^+ yrast state belonging to the $K^\pi = 0^+$ rotational band based on the ground state. The data from the ^{11}B(^{13}C,d) clearly confirm this assignment.

As can be seen from the fig. 6a the 4.46 MeV and 5.14 MeV angular distributions are fitted by angular distributions of spin 2. Endt et al.[24] listed them as being 2^+ and 2^- respectively. However in this case our method is insensitive to the parity of the final state.

The most important discrepancy between our results and the previously assigned spin values is related to the 5.52 MeV state. The study of ^{19}F(α,pγ)^{22}Ne angular correlation performed by Neogy et al.[25] indicates a pure $\ell = 2$ transition to this state, restricting the spin and parity assignment to 3^+ or 4^+. On the other hand, on the basis of α scattering experiments on ^{22}Ne[31] it has been found that this state should have natural parity and a 4^+ assignment being acceptable. However this assignment cannot be supported by our data on the basis of the statistical model calculations, that suggest a J = 3 value for this level. According

to the shell model predictions by Preedom and Wildenthal[5], J = 3 and J = 4 spin levels are expected between 5.40 MeV and 5.50 MeV. The best fit to the 5.64 MeV state is obtained for J = 3; in that case the 5.52 MeV state would be the best candidate for the J = 4 state.

6.30 MeV and 6.34 MeV: The 6.30 MeV level is listed in ref. 22 as the 6^+ yrast state and the 6.34 MeV as a $J^\pi = 4^+$ state, based on the work of Fifield et al.[13]. In the present work, it was not possible to resolve this doublet, however our best fit is for a sum 6 + 4. The best χ^2 fit to the shape of the angular distribution is obtained for spin 6 (fig. 7).

Unresolved doublets were observed at 6.64 MeV, 6.82 MeV, 7.34 MeV and 7.40 MeV. Fits using several combinations of spin were used and the best χ^2 values were obtained for the spin values suggested in references 12, 13, 24. We should note that the lowest I = 5 value is attributed to the 7.35 MeV state although this suggestion is not supported by previous assignments.

7.72 MeV, 7.92 MeV and 8.08 MeV: The statistical analysis results for these states agree with the spin values listed in references 12, 13, 24 with the exception of the 7.92 MeV for which the best χ^2 fit to the angular distribution is for a spin 3 (the possibility of being a doublet J = 2 + 2 is not ruled out).

Endt and Van der Leun[24] listed a state at 8.131 MeV, $J^\pi = 2^+$ and another at 8.162 MeV, $J^\pi = 3$. We observed a state at 8.14 MeV which is probably a doublet either a J = 4 + 3 or J = 4 + 2.

The 8.38 MeV, 8.50 MeV and 8.59 MeV states were very difficult to analyse due to superposition. The experimental FWHM of this cluster suggests that probably there are more than three peaks. In such cases the shape of the angular distribution was

also fitted indicating a spin J = 4 at 8.38 MeV and a spin J = 5 at 8.50 MeV and 8.59 MeV.

8.74 MeV: In the present work, the high absolute cross section value together with the high anisotropy of the angular distribution indicate a multiplet of lower spins. The best χ^2 fit to the shape of the angular distribution is obtained for a spin J = 3. This suggestion is supported by ref. 24.

The observed levels between 9.0 MeV and 10.0 MeV presented no problems concerning the fitting procedure. Our assignments were not in conflict with the few previous suggestions when they were available.

In the region of 10.0 to 11.0 MeV in excitation energy, Broude et al.[12] reported two spin 5 states at 10.64 and 10.76 MeV respectively and a J = 6,8 at 10.4 MeV. In this work two spin J = 6 states were observed in that region, but a little higher in excitation energy, when compared to Broude[12] assignment, at 10.66 and 10.78 MeV. Our suggestion, however is in better agreement with Arima et al.[4] prediction of a state of spin J = 6 near 11.0 MeV excitation energy. We observed a spin state J = 5 at 10.31 MeV, a spin J = 7 at 10.42 MeV and a probable doublet of spins 4 + 3 at 10.19 MeV. Our J = 5 suggestion is 300 keV lower in excitation energy than Broude et al.[12] assignment of a state of spin J = 5 at 10.64 MeV, but can be compared with Arima et al.[4] prediction of a spin state J = 5 at 10.50 MeV.

Between 11.00 and 12.00 MeV excitation energy we observed two spin 7 states and two spin J = 6 besides the yrast J = 8 at 11.02 MeV. In the same region Arima[4] predicts the yrast J = 8 at 11.2 MeV, and two states with J = 6. The 6^+ state predicted by Arima[4], at ∿ 11.7 MeV could be associated with one of our

suggestions: at 11.64 MeV or 11.74 MeV. Broude et al.[12] observed a level at 11.1 MeV for which has been assigned 6, 7 or 8.

Above 12.00 MeV of excitation energy there is no other experimental data for high spin states available in the literature. In this case our results can be compared only with theoretical predictions.

As can be seen in fig. 10, the second J = 8 is predicted by Wildenthal[5] at 12.6 MeV and by Arima[4] at 12.1 MeV; in the present work the second spin J = 8 was observed at 13.00 MeV excitation energy.

From 12.00 to 13.00 MeV in excitation energy we observed a number of levels, but spin assignments were not possible for all of them due to fitting problems arising from the superposition of peaks. For the peaks we could analyse, we assigned two spins J = 6, at 12.17 and 12.33 MeV, and two spins J = 7 at 12.04 and 12.39 MeV. The level at 12.04 MeV, J = 7 observed in this work could be associated with Wildenthal's[5] prediction of a spin 7^+ at 11.9 MeV excitation energy. The predictions of Arima et al.[4] for this energy interval do not show a perfect agreement our observations: apart from the J = 8 at 12.1 MeV mentioned above, he suggests a spin J = 6 at 12.95 MeV and a spin J = 5 at 12.8 MeV.

Above 13.0 MeV excitation energy, most of the ^{22}Ne high spin states observed in the present work cannot be compared even with theoretical predictions which are very rare.

Preedom et al.[5] predicted a $I^\pi = 9^-$ state at 15.5 MeV and $I^\pi = 10^+$ state at 16.35 MeV excitation energy. Arima et al.[4] found a 9^- state at E* = 14.5 MeV, and 15.6 MeV for the 10^+ state that would lead to a predicted backbending in the ^{22}Ne yrast line. This last prediction has been confirmed by the present work

(I* = 10 at E* = 15.46 MeV). The first I = 9 state is suggested, at 17.7 MeV. However this transition correspond to a doublet. The fit of the shape and magnitude of the angular distribution indicated a [9 + (4,5)] doublet.

V. THE ^{22}Ne STRUCTURE

In contrast to heavier nuclei, very reliable nuclear structure calculations are available[1,4,5] for s-d nuclei, and can be applied in the description of experimental eveidences. Very important features are related to the behaviour of these nuclei under strong centrifugal and Coriolis forces during fast rotational conditions leading sometimes to phenomena like backbending etc.. This mass region is best suited for the confrontation of the complete-microscopic-shell-model calculations with the macroscopic descriptions, i.e, the Strutinsky procedure.

The lack of systematic experimental information in ^{22}Ne did not allow to establish a clear and acceptable description of the ^{22}Ne structure as it has been made in the cases of ^{20}Ne[10], ^{22}Na[36], ^{23}Na[37,38] and ^{24}Mg[10,11]. Therefore, the comparison of the present results with the predictions of all the available models of s-d shell nuclei can bring a better understanding of the behaviour of these light nuclei under fast rotation.

The first important feature observed in the ^{22}Ne yrast line, is the backbending, around spin 8, previously reported[14], and depicted in fig. 11. The theoretical shell model predictions for the ^{22}Ne are presented in fig. 10 whereas the results of the

application of the Strutinsky procedure to ^{22}Ne are shown in fig. 12[14].

The first important point we would like to discuss is the drastic increase of the moment of inertia of ^{22}Ne when compared to ^{20}Ne (see fig.11). This difference is larger by much more than can be accounted for by a simple $A^{5/3}$ scaling of the moments of inertia. For the 6^+ state in ^{20}Ne $\mathcal{J}^{20}_{6^+} \sim 4.83$ MeV^{-1} and a value of $\mathcal{J}^{22}_{6^+} \sim 5.67$ MeV^{-1} should be expected. However a $\mathcal{J}^{22}_{6^+} \sim 6.37$ MeV^{-1} value has been obtained experimentally. It is interesting to notice that the experimental moment of inertia of ^{21}Ne for the $15/2^+$ state is ~ 5.65 MeV^{-1} instead of ~ 5.24 MeV^{-1} expected from a $A^{5/3}$ scaling. However the 5.65 MeV^{-1} value is not in conflict with the ^{22}Ne moment of inertia constant value.

These results could be in conflict with the expectation of a lower deformation for T = 1 nuclei (^{22}Ne), when compared to a T = 0 nucleus (^{20}Ne). The experimental evidence could be explained in terms of a strong coupling of the first neutron to the ^{20}Ne case, leading to ^{21}Ne, with a higher polarization and increasing substantially the moment of inertia. When a second neutron is coupled in, the pairing interaction does not allow a drastic increase of $\mathcal{J}^{22}$ compared to $\mathcal{J}^{21}$.

A similar interpretation has been given by Grümmer et al.[15] that describes the increase of $\mathcal{J}_I$ with I (and ω^2), for small values of I, in ^{22}Ne as a consequence of the blocking effect, which reduces the possibility of pairing correlations already for small values of I. He shows that the spectrum of ^{22}Ne for $I \leq 6$ is governed by the strong decrease of the pairing correlations, whereas for higher I the states are merely uncorrelated. Such an antipairing effect is believed to be responsible for the strong anomaly in the moments

of inertia for the high spin states, i.e., backbending of the yrast line. Grümmer et al.[14] proposed that the slight decrease of the moment of inertia between spins 6^+ and 8^+ is correlated with a decrease of the quadrupole deformation with increasing angular momentum, denominated antistretching. Still according to them this antistretching is connected with the low band cut-off values in the s-d shell[39,40].

This picture leads to a break-down of the clear rotational behaviour which is possibly connected with the low band cut-off values in the s-d shell.

For a typical s-d shell nucleus like ^{22}Ne the number of s-d shell configurations for $J \geq 6$ becomes noticeably smaller than for lower J values and is only six for J = 10, which is the maximum J value and therefore necessarily the end of the rotational band in a microscopic description[14]. As a consequence, the higher rotational states near the band cutoff are not collective enough to preserve the characteristics of a rotor and occurs the antistretching.

This description is somehow in agreement with the results of the Strutinsky type calculations (see fig. 12), performed by Mosel et al.[14]. The sharp minima with respect to β deformations in the β-γ deformation-energy surface show a drastic antistretching effect mainly in ^{20}Ne up to spin 14, simultaneous with the trend towards triaxiality. On the other hand, the softness of the minima in the β-γ plane with respect to the γ deformation in contrast to the case of "good" heavy rotors explains the experimental difficulties in defining excited rotational states in ^{22}Ne.

Another difference between ^{20}Ne and ^{22}Ne observed in fig. 12 is correlated with a later approach to $\gamma = -60^\circ$ in the ^{22}Ne case, corresponding to an oblate nucleus rotating around the

symmetry axis. In this state all particles in the open s-d shell are aligned along the rotation axis. Naturally, this alignment takes place later in ^{22}Ne because of the two extra nuclei.

In spite of the expected difficulties in defining rotational bands in ^{22}Ne, the nuclear shell model, by means of residual forces, has been able to induce strong configurations mixings which can sometimes be interpreted as rotational motions.

ACKNOWLEDGEMENTS

The authors are grateful to Prof. U. Mosel for the collaboration in the theoretical calculations and to Prof. O. Sala for the enlightning discussions.

REFERENCES

1. A. Watt, D. Kelvin and R.R. Whitehead, Phys.Lett. 63B (1976) 385 and Phys.Lett. 63B (1976) 388; R.R. Whitehead, A. Watt, B.J. Cole and I. Morrison, Adv.Nucl.Phys. 3 (1977) 123.

2. K. Neegård, V.V. Pashkevich and S. Franendorf, Nucl.Phys. A262 (1976) 61; G. Anderson, S.E. Larson, G. Leander, P. Möller, S.G. Nilsson, R. Bengtsson, J. Dudek, B. Nerlo-Pomorska, K. Pomorsky and Z. Szymansky, Nucl.Phys. A268 (1976) 205.

3. D. Glas and U. Mosel, Phys.Lett. 78B (1978) 9.

4. Y. Akiyama, A. Arima and T. Sebe, Nucl.Phys. A138 (1969); A. Arima, M. Sakakura and T. Sebe, Nucl.Phys. A170 (1971) 273.

5. B.M. Preedom and B.H. Wildenthal, Phys.Rev. C6 (1972) 1633; and Proceedings on the 5th Symposium on Nuclear Structure of Low-medium-mass Nuclei - Univ.of Kentucky Press (1973).

6. E.C. Halbert, J.B. McGrory, B.H. Wildenthal and S.P. Pandaya, Advances in Nuclear Physics, vol. 4 ed. M. Baranger and E. Vogt (Plenum Press, New York 1971) p. 315.

7. G. Craig, Nucl.Phys. A225 (1974) 493.

8. A. Faessler, Lectures given at the XI International School on Nuclear Physics, August 1976, Predeal, Romania.

9. F.S. Stephens, Rev.Mod.Phys. 47 (1975) 43; Lecture Notes in Physics 92 (1979) 117, edited by B.A. Robson (Springer-Verlag).

10. L.K. Fifield, R.W. Zurmühle, D.P. Balamuth and J.W. Noé, Phys. Rev. C8 (1973) 2203; H.T. Fortune, Proc.Int.Conf. Nuclear Structure, Tokyo (1977) 99; J.Phys.Soc. Japan 44 (1978).

11. A. Szanto de Toledo, M. Schrader, E.M. Szanto, G. Rosner, H. V. Klapdor, Phys.Lett. 78B (1978) 58; Nucl.Phys. A315 (1979) 500 and H.V. Klapdor, Lectures Notes in Physics 92 (1979) 125.

12. C. Broude, W.G. Davies, J.S. Forster and G.C. Ball, Phys.Rev. C13 (1976) 953.

13. L.K. Fifield, R.W. Zurmühle, D.P. Balamuth and S.L. Tabor, Phys.Rev. C13, nº 4 (1976) 1515; Phys.Rev. C10 (1974) 1785.

14. E.M. Szanto, A. Szanto de Toledo, H.V. Klapdor, M. Diebel, J. Fleckner and U. Mosel, Phys.Rev.Lett. 42 (1979) 622.

15. F. Grümmer, K. Goeke, K. Allaart, A. Faessler, Nucl.Phys. A225 (1974) 443.

16. G. Rosner, Ph.D. Thesis, Max-Planck-Institut,Heidelberg (1977) unpublished.
M. Schrader, M.P.I. Jaresbericht 1977, pg 41 (unpublished)

17. T.D. Thomas, Ann.Rev.Nucl.Sc. 18 (1968) 343.

18. T. Ericson, Ann. of Phys. 23 (1963) 390.
T. Ericson and T. Mayer-Kuckuk, Ann.Rev.Nucl.Sci. 16 (1966) 183.

19. A. Gilbert and A.G.W. Cameron, Can.J.Phys. 43 (1965) 1446.

20. U. Facchini, E. Saetta, Menichella, Energia Nuclear 15, nº 1 (1963) 53.

21. R.G. Stokstad, Wright Nuclear Structure Laboratory, Yale University, Internal Report nº 52, 1972 (unpublished).

22. D.G. Kovar et al., Phys.Rev. C20 (1979) 1305.

23. A. Szanto de Toledo, M. Schrader, E.M. Szanto, H.V. Klapdor, Phys.Rev. C19 (1979) 555.

24. P.M. Endt and c. Vand der Leun, Nucl.Phys. A310 (1978) 1.

25. P. Neogy, R. Middleton and W. Scholz, Phys.Rev. C6, nº 3 (1972) 885.

26. R.W. Ollerhead, G.R.F. Allen, A.M. Baxter, W.J. Gillespie and J.A. Kuehner, Bull.Am.Phys.Soc. II 14 (1969) 1221.

27. C.N. Davids, D.R. Goosman, D.E. Alburger, A. Gallmann, G. Guillaume, D.H. Wilkinson and W.A. Lanford, Phys.Rev. C9, 1 (1974) 216.

28. A.J. Howard, R.G. Hirko, D.A. Bromley, K. Bethge and J.W. Olness, Nuovo Cimento 11A (1972) 575.

29. W. Kutschera, D. Pelte and G. Schrieder, Nucl.Phys. A111 (1968) 550.

30. X.K. Maruyama, R.A. Lindgren, W.L. Bendel, E.C. Jones Jr. and L.W. Fagg, Phys.Rev. C10 (1974) 6.

31. S. Buhl, D. Pelte and B. Povh, Nucl.Phys. A91 (1967) 319.

32. D. Pelte, B. Povh and W. Scholz, Nucl.Phys. 52 (1964) 333.

33. W. Scholz, P. Neogy, K. Bethge and R. Middleton, Phys.Rev. C6 nº 3 (1972) 893.

34. W. Oelert, W. Chung, A. Djaloeis, C. Mayer, Böricke and P. Turek, Phys.Rev. C22, nº 2 (1980) 408.

35. C.M. Perey and F.G. Perey, Atom.Data Nucl. Data Tab. 13, 4 (1974) 294; 10 (1972) 539.

36. J. Gomez del Campo, J.L.C. Ford Jr., R.L. Robinson, P.H. Stelson and S.T. Thornton, Phys.Rev. C9, nº 4 (1974) 1258.

37. J. Gomez del Campo, D.E. Gustafson, R.L. Robinson, P.H. Stelson, P.D. Miller, J.K. Blair and J.B. McGrory, Phys.Rev. C12, nº 4 (1975) 1247.

38. D.E. Gustafson, S.T. Thornton, T.C. Schweizer, J.L.C. Ford Jr., P.D. Miller, R.L. Robinson and P.H. Stelson, Phys.Rev. C13 nº 2 (1976) 691.

39. G. Goeke, J. Garcia and A. Faessler, Nucl.Phys. A208 (1973) 447.

40. Y. Abgrall, B. Morand and E. Courier, Nucl.Phys. A192 (1972) 373.

TABLE I - Averaged excitation energies obtained in the present work for ^{22}Ne (energies indicated with asterisc where used as references for energy calibration).

E^*(MeV)[a]	J^{π}[a]	E^*(MeV)[b]	J^b	$\langle d\sigma/d\Omega\rangle_{exp}(\theta_{LAB}=13^o)$ (μb/sr)[b]
0	0^+			
1.27457	2^+	1.28		
3.3572*	4^+	3.36	4	
4.4567*	2^+	4.46	2	.95
5.1475*	2^-	5.14	2	1.44
5.336*	1^+	5.34	2+1	1.18
5.365*	2^+			
5.5232*	4^+	5.52	3	1.10
5.6413*	3^+	5.64	3	1.97
5.9099*	3^-	5.91	2+3	
6.115*	2^+	6.12	2	1.21
6.237	0^+			
6.3114*	6^+	6.31	6+4	12.39
6.3452*	4^+			
6.6360*	$(2,3)^+$	6.66	3+3	3.29
6.691*	1^-			
6.817*	2^+	6.84	2+1	1.82
6.854*	1^+			
6.904	$(0,1)^+$			

E^* (MeV)[a]	J^{π}[a]	E^* (MeV)[b]	J[b]	$\langle d\sigma/d\Omega\rangle_{exp}(\theta_{LAB}=13^{\circ})$ (μb/sr)[b]
7.052*	1^-	7.05		1.69
7.341*	$(3,4)^+$	7.34	5+3	8.63
7.342*	0^+			
7.406*	$(1,3)^-$	7.42	4+3	5.82
7.423*	$(3,5)^+$			
7.470*				
7.489	1^-	7.54		1.48
7.644*	2^+	7.64		4.08
7.664	2^-			
7.721*	3^-	7.72	3	1.95
7.924*	2^+	7.92	3	1.90
8.081*	$(2-4)^+$	8.08	3	1.74
8.131*	2^+	8.14	4+3	5.38
8.162	3			
8.382*	$(3^-,4^+)$	8.38	4	3.50
8.491*	2^+	8.50	5+4	9.39
8.548	$(0-4)^+$			
8.592*		8.58		8.52
8.737	3^-	8.74	5	9.48
8.861	$(0-4)^+$	8.89		1.69
8.902	$(0-3)^-$			
8.979*		8.97		2.06
9.040				
9.097*	$(1-3)^-$	9.07	4+3	4.87
9.170*		9.18	5	6.94
9.223				
9.250				
9.325*		9.34		7.69
		9.50	5	5.10
		9.64	4+3	3.94
		9.72	6	10.85
		9.86	5	6.85
		10.12		3.65
		10.19	4	3.21
		10.31	5	5.00
		10.42	7	12.73
10.616*		10.66	6	10.60
10.750*		10.78	6	9.83
10.854				
10.920				
		11.02	8	26.34
11.193		11.14	7	
11.267		11.26	7.8	2.95
11.435				
11.464	1^-			
11.519		11.50		33.19

E^* (MeV)[a]	J^{π}[a]	E^* (MeV)[b]	J^b	$\langle d\sigma/d\Omega\rangle_{exp}(\theta_{LAB}=13^o)$ (μb/sr)[b]
11.578				
11.686	2^+	11.64	6	14.72
11.746		11.74	6	8.90
11.752	1^-			
11.886	1^-	11.87		6.58
11.92	2^+			
12.04	0^+	12.04	7	12.87
12.056				
		12.12		12.74
		12.17	6	8.87
12.25	0^+			
12.28	1^-			
		12.33	6	10.68
12.38	2^+	12.39	7	17.14
12.48	(2^+)			
12.58	1^-	12.56		6.19
12.61	$(1^-,2^+)$			
		12.69		20.23
12.81	2^+			
12.83	1^-			
12.88	3^-	12.88		25.64
		13.00	8	28.44
		13.26	7	17.00
		13.47	6	7.94
		13.72	7	15.79
		13.79		
		13.88	8	23.26
		14.03	7	20.97
14.07				
		14.13		7.35
		14.23		10.81
		14.34		8.15
		14.42		4.50
		14.54		6.13
		14.60		7.84
		14.69		8.90
		14.84	7	10.86
		14.91	7	13.58
		15.25	6	11.70
		15.35	7	12.19
15.400				
		15.46	10	30.77
		15.57		8.28
15.610				
		15.67	7	16.87
		15.80	8	21.31

E^* (MeV)[a]	$J^{\pi a}$	E^* (MeV)[b]	J^b	$\langle d\sigma/d\Omega\rangle_{exp}(\theta_{LAB}=13^o)$ (μb/sr)[b]
		15.99	8	26.48
		16.05	7	13.47
16.06				
		16.25	6, 5+5	8.83
		16.38		9.05
		16.45		10.16
		16.53	7, 6+5	11.44
		16.61	6	8.27
		16.74	7	13.27
		16.88	7	16.69
		17.03	7, 6+5	6.90
		17.20	8	17.73
		17.39	8	20.00
		17.48		13.07
		17.58	8	18.13
		17.76	9+4	22.95
		18.01		
		18.08		
		18.17		
		18.28		

a) Values obtained from reference 24.

b) Present work.

TABLE II - Optical model parameters and parameters used in the Hauser-Feshbach calculations for the $^{11}B + ^{13}C$ reaction

	$^{11}B+^{13}C$	$^{23}Ne+p$	$^{23}Na+n$	$^{22}Ne+d$	$^{20}F+\alpha$	$^{21}F+^3He$
a	2.33	4.12	4.12	3.94	3.86	3.76
Δ (MeV)	3.94[a]	2.88[a]	2.67[b]	5.90[a]	0.0	2.67[b]
V (MeV)	100.0	49.1	52.0	50.0	105.1	186.0
r_0 (fm)	1.01	1.10	1.22	1.3	1.496	1.07
a_0 (fm)	0.70	0.63	0.52	0.55	0.511	0.72
W (MeV)	26.0[v]	6.6[s]	3.12[v]	13.0[v]	15.45[v]	18.0[v]
r_W (fm)	1.08	1.34	1.22	1.3	1.496	1.60
a_W (fm)	0.44	0.6	0.52	0.55	0.511	1.04
r_{yrast} (fm)	1.34	1.34	1.34	1.34	1.34	1.34

Optical model parameters obtained from reference 35

a) from reference 19

b) from reference 17

v) volume imaginary potential

s) surface imaginary potential (Wood-Saxon derivative)

FIGURE CAPTIONS

Figure 1. Grazing Collision Picture for the $^{11}B(^{13}C,d)^{22}Ne$ reaction using semiclassical expressions for yrast line and grazing angular momenta determination[11].

Figure 2. a) Typical spectrum obtained for the $^{11}B(^{13}C,d)^{22}Ne$ (E_{LAB} = 41.36 MeV; θ_{LAB} = 13°)

b) Typical spectrum obtained for the $^{13}C(^{11}B,d)^{22}Ne$ (E_{LAB} = 35 MeV; θ_{LAB} = 20.5°)

Figure 3. Typical fit obtained with the peak-fitting program JASPER[15] for the $^{11}B(^{13}C,d)^{22}Ne$ (θ_{LAB} = 5.5°) spectrum (Uncertainties originated by the choice of different polinomials for the background definition were taken into account in the cross-section uncertainty).

Figure 4. Left: Partial cross-sections $\sigma_J(E^*,I)$ for the population of final states (E^*,I = 0,2,...,14) as a function of compound nucleus angular momentum.

Right: Total cross section $\sigma_{J_{max}}(E^*,I)$ as a function of the truncation value J_{max}.

$$\sigma_{J_{max}}(E^*,I) = \sum_{J=0}^{J_{max}} \sigma_J(E^*,I)$$

Figure 5. Angular distributions anisotropy (R) predicted by statistical model calculations as a function of the final state angular momentum I, for different values of J_{max}.

Figure 6. a-f

Experimental angular distributions for the $^{11}B(^{13}C,d)$ and $^{13}C(^{11}B,d)^{22}Ne$ reactions. Theoretical angular distributions were calculated for several I values and are presented with their correspondent χ^2 values. Thick curves correspond to I-values previously determined and compiled in reference 22.

Figure 7. a) Left: χ^2 of fits to the absolute angular distributions by statistical model calculations as a function of the spin of the final state (assuming singlets). The 6^+ yrast state at 6.30 MeV has been fitted also together with the unresolved 4^+ state at 6.34 MeV.

b) Right: χ^2 of fits to the shape of the angular distributions by statistical-model calculations as a function of the spin of the final state.

Figure 8. Effective number of channels (calculated with the code STATIS) as function of the center of mass angle for different spin final states.

Figure 9. Experimental level scheme obtained from the present work (P) and from the literature (R; ref. 10,24).

Figure 10. Theoretical level scheme base on calculations presented in ref. 4(A); ref. 5(B), ref. 10(C).

Figure 11. Effective moment of inertia plotted as a function of the square of the effective rotational frequencies for ^{20}Ne and ^{22}Ne.

Figure 12. Trajectories in the β-γ deformation energy surfaces for yrast states in ^{20}Ne and ^{22}Ne.

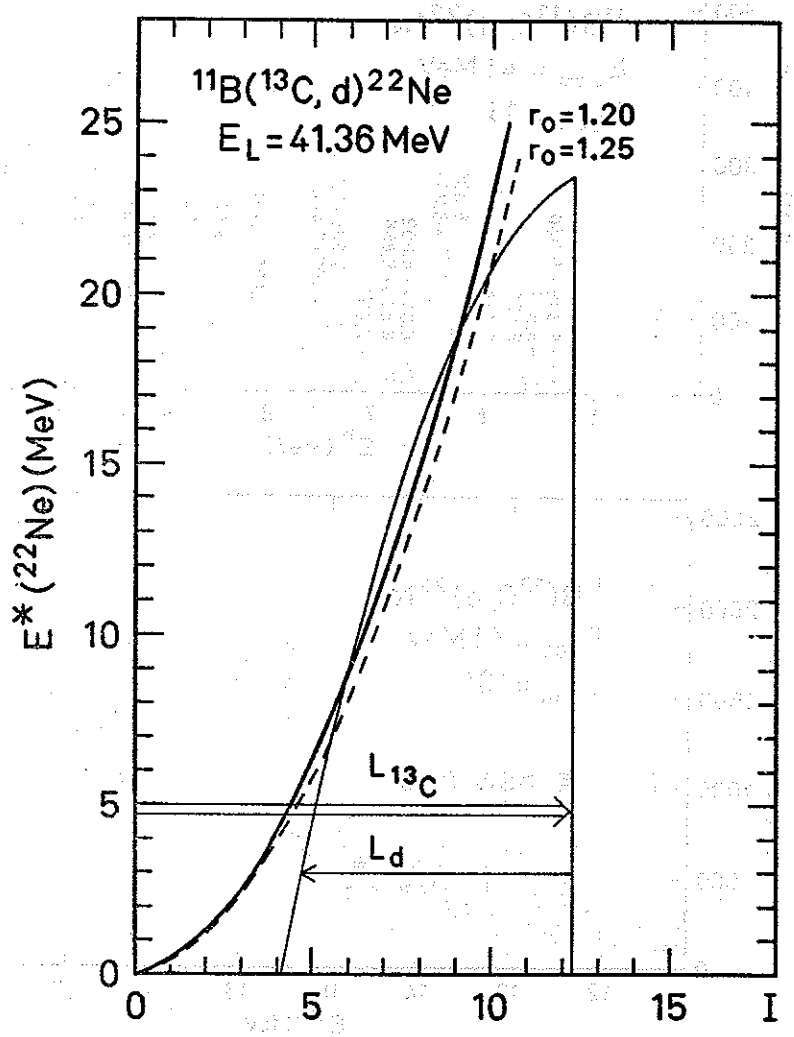

FIGURE 1

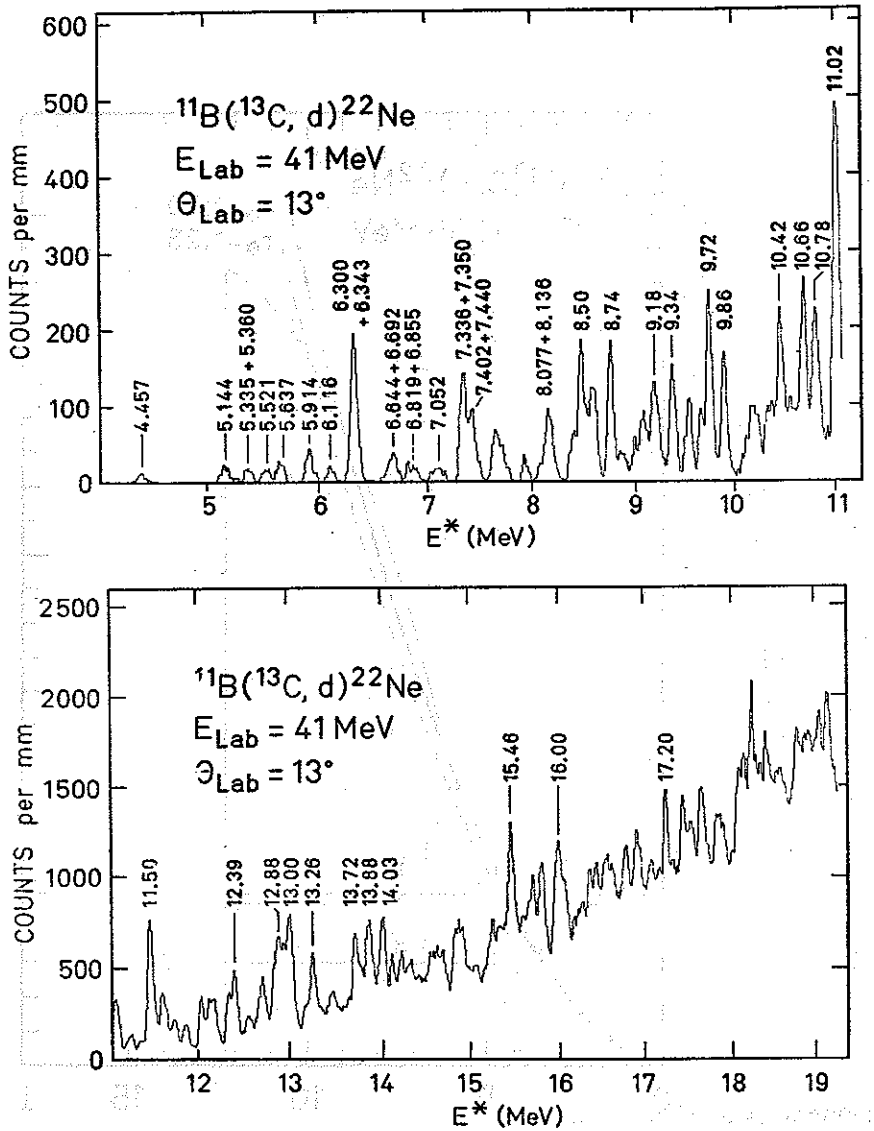

FIGURE 2 a.

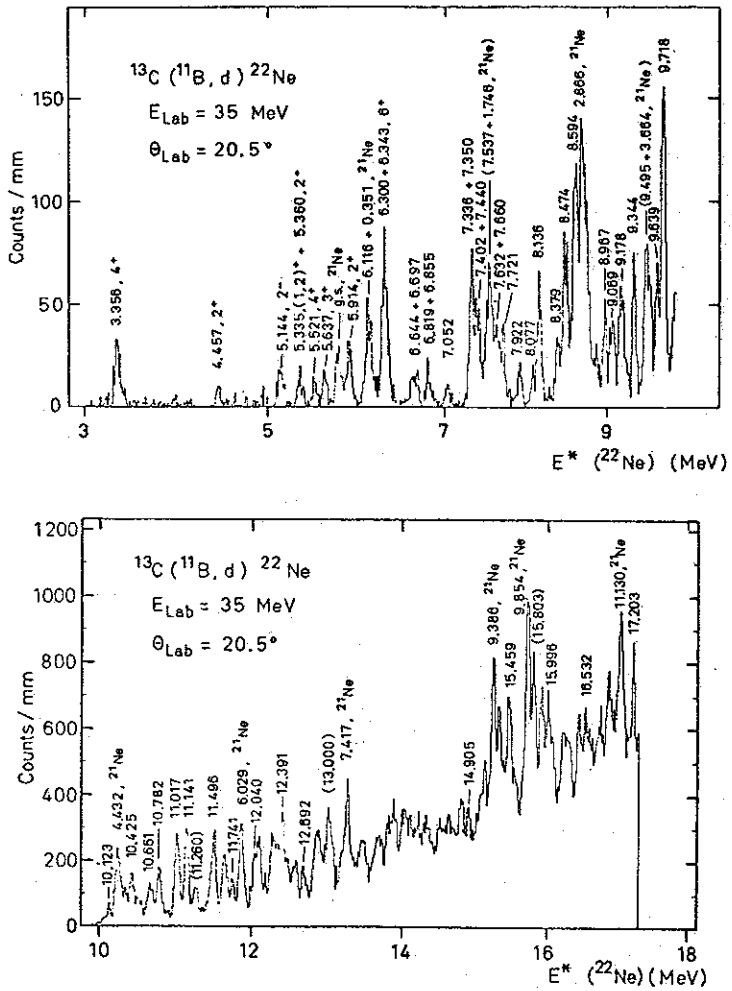

FIGURE 2b

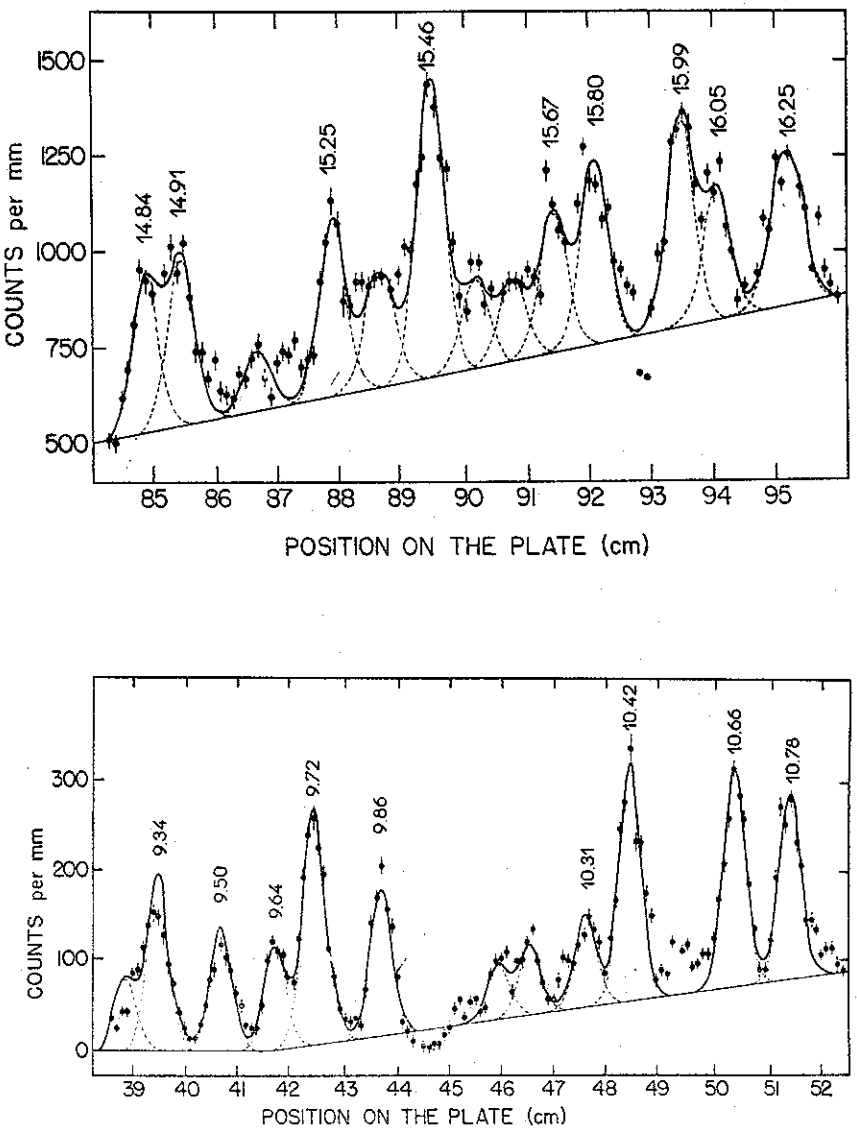

FIGURE 3

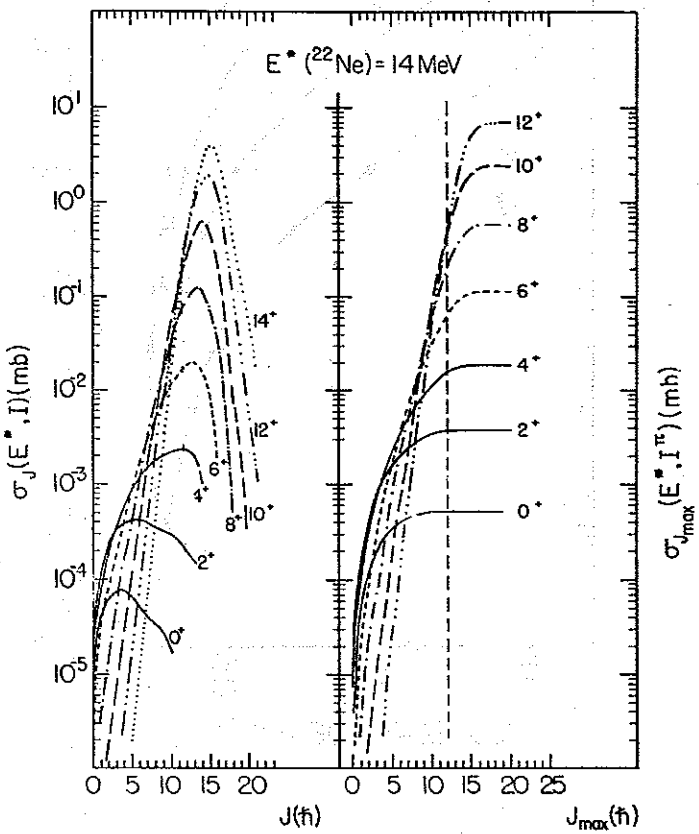

FIGURE 4

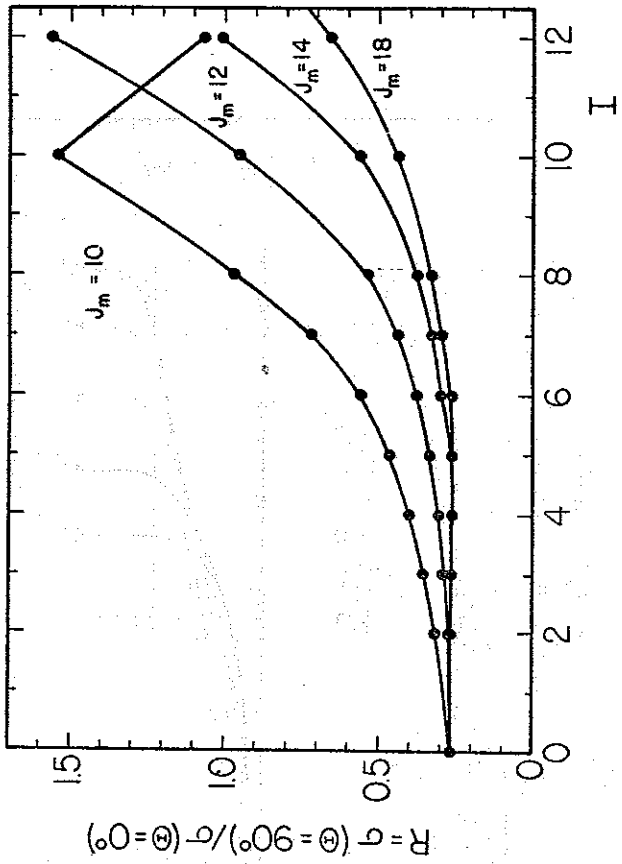

FIGURE 5

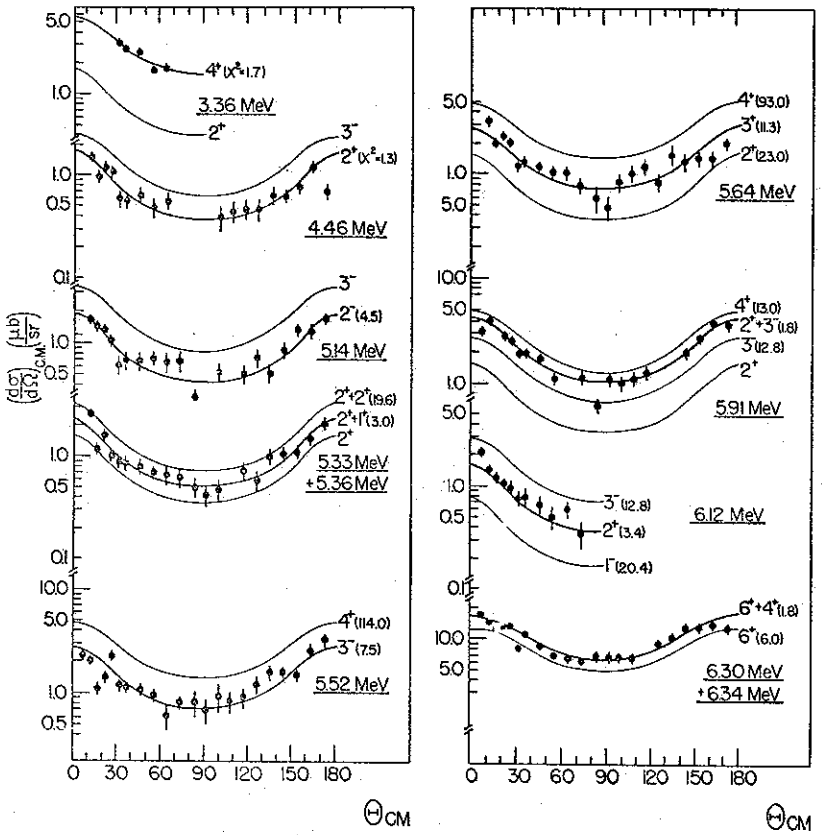

FIGURE 6a

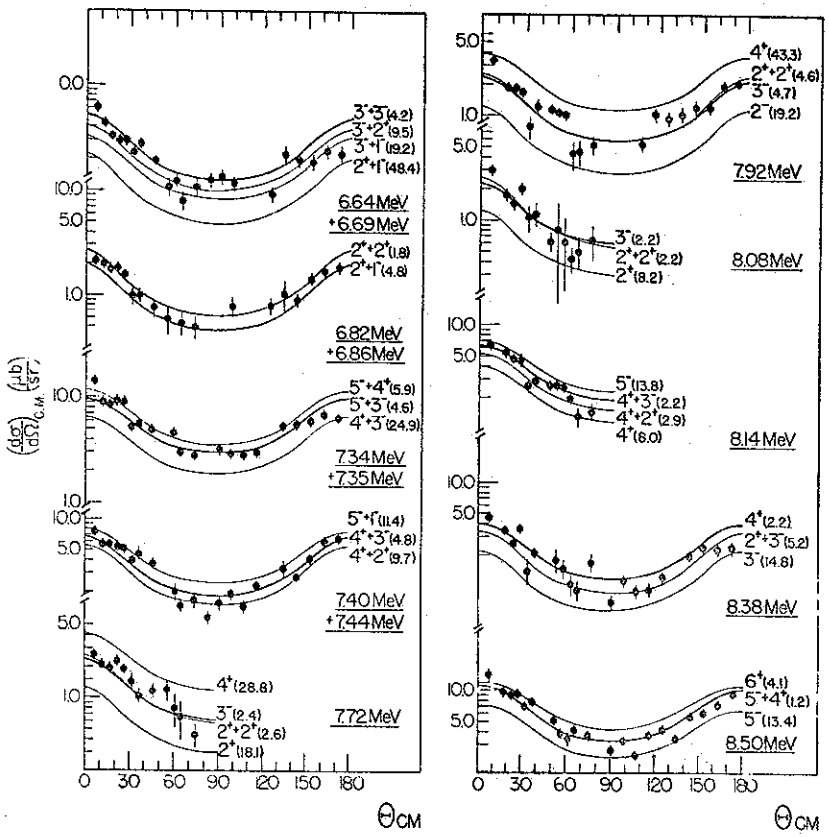

FIGURE 6b

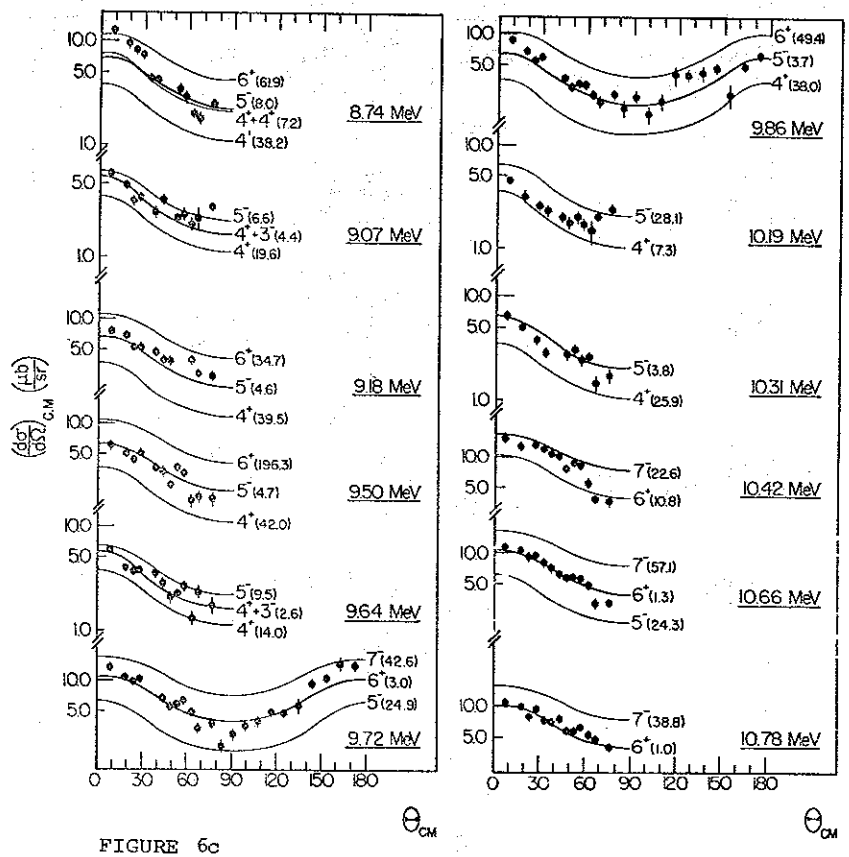

FIGURE 6c

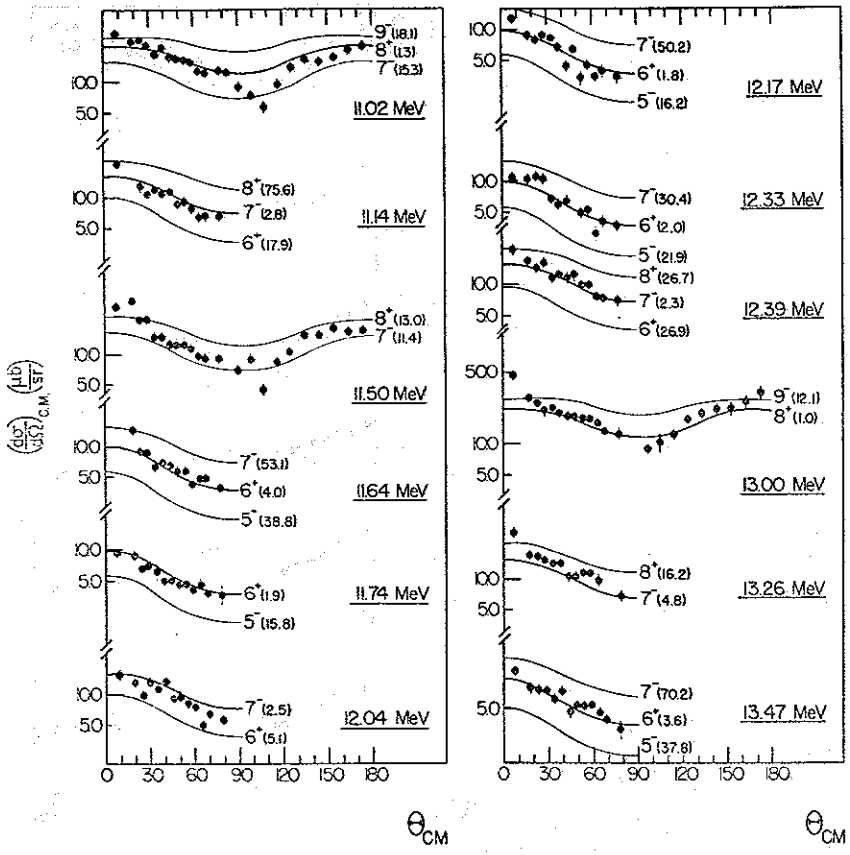

FIGURE 6d

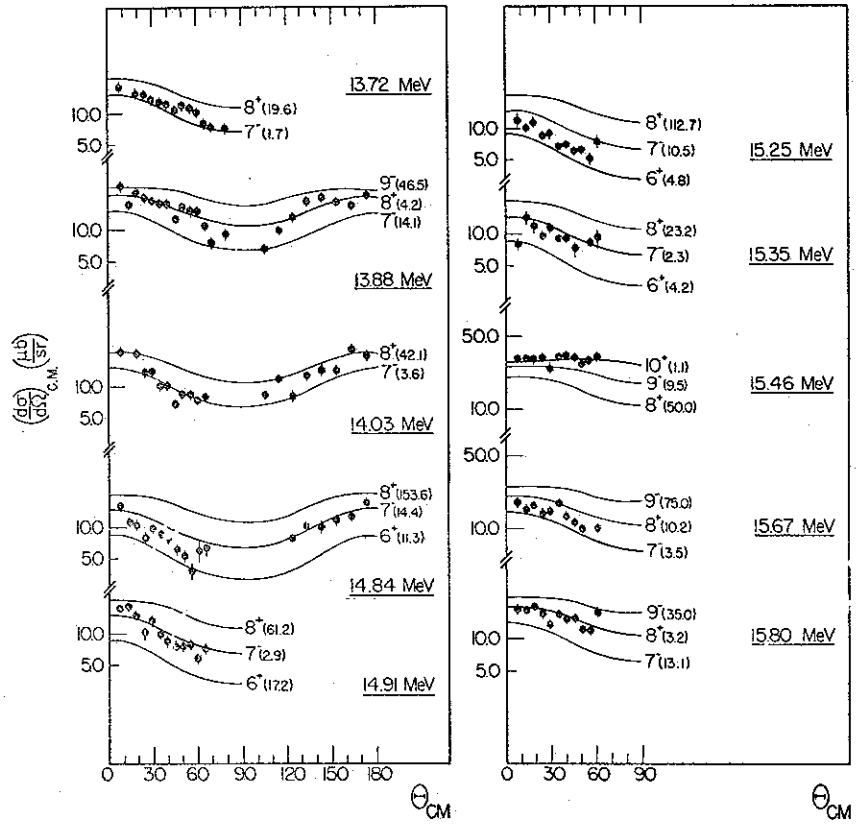

FIGURE 6e

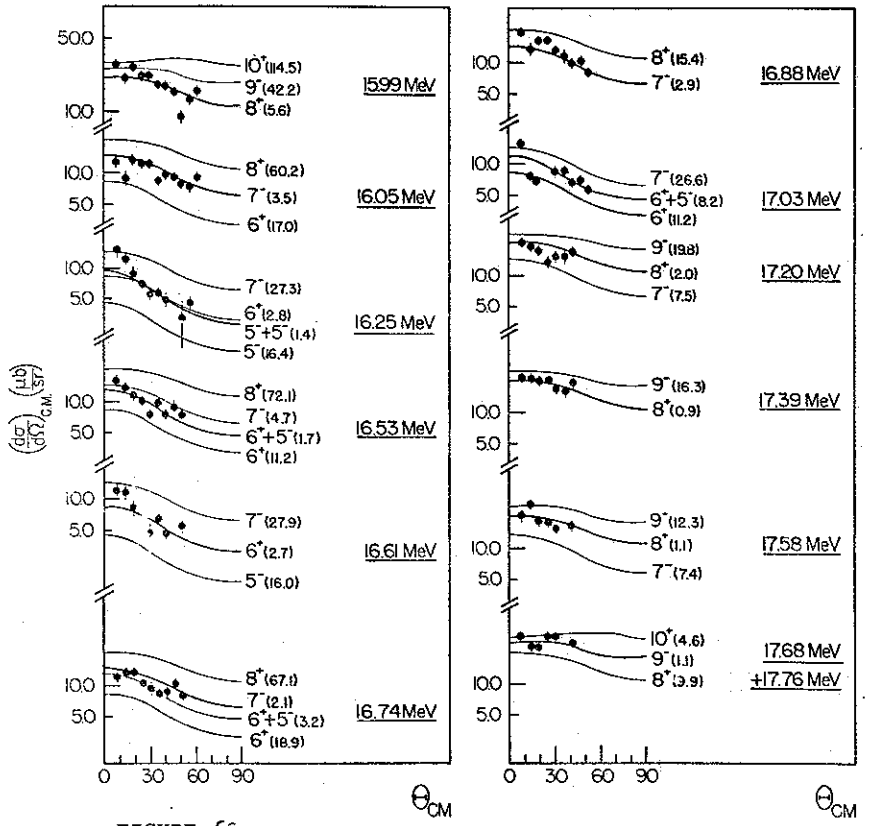

FIGURE 6f

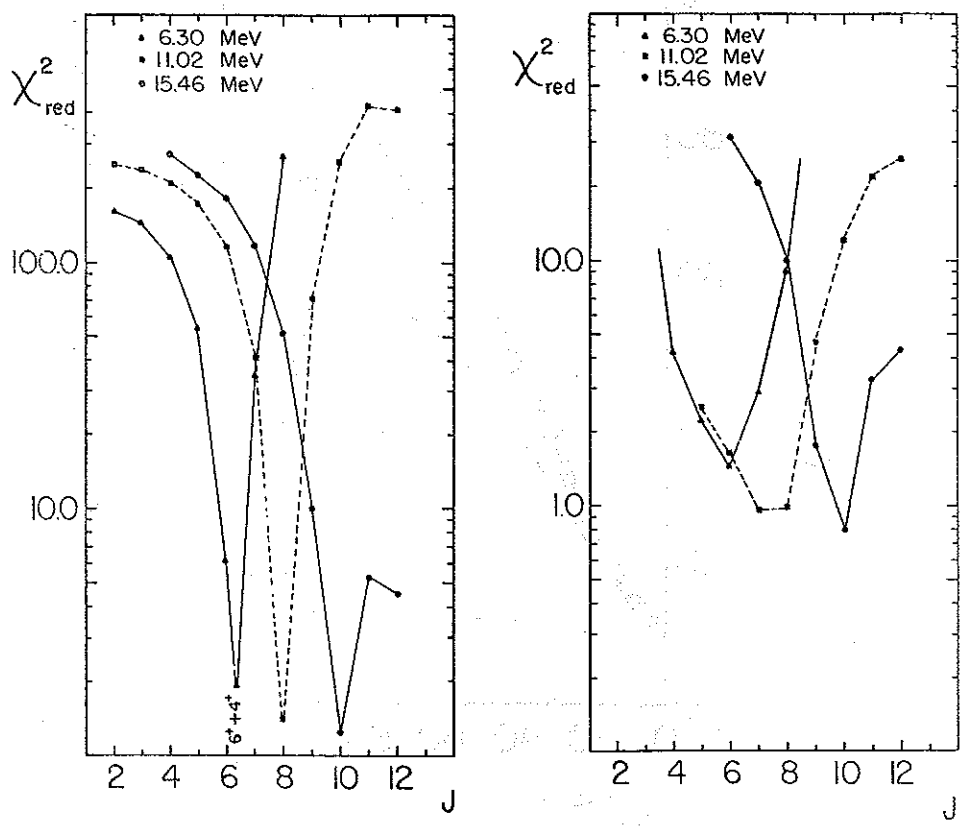

FIGURE 7

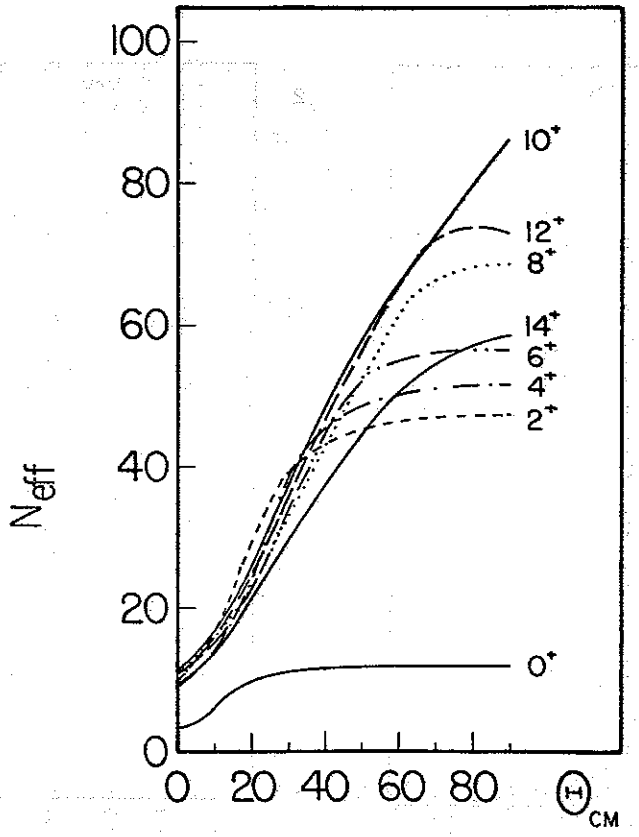

FIGURE 8

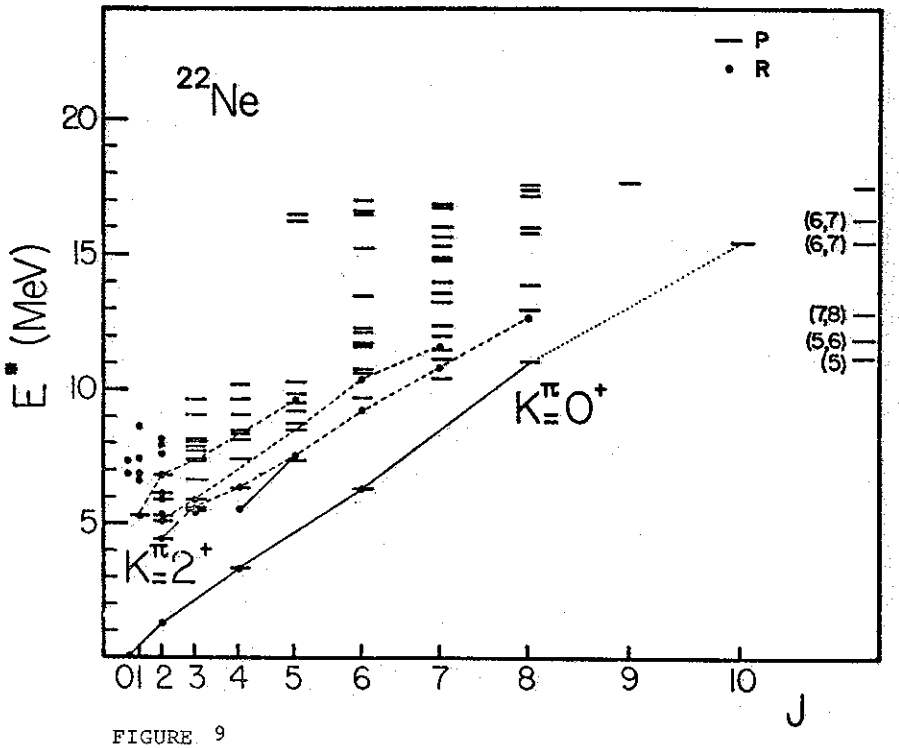

FIGURE 9

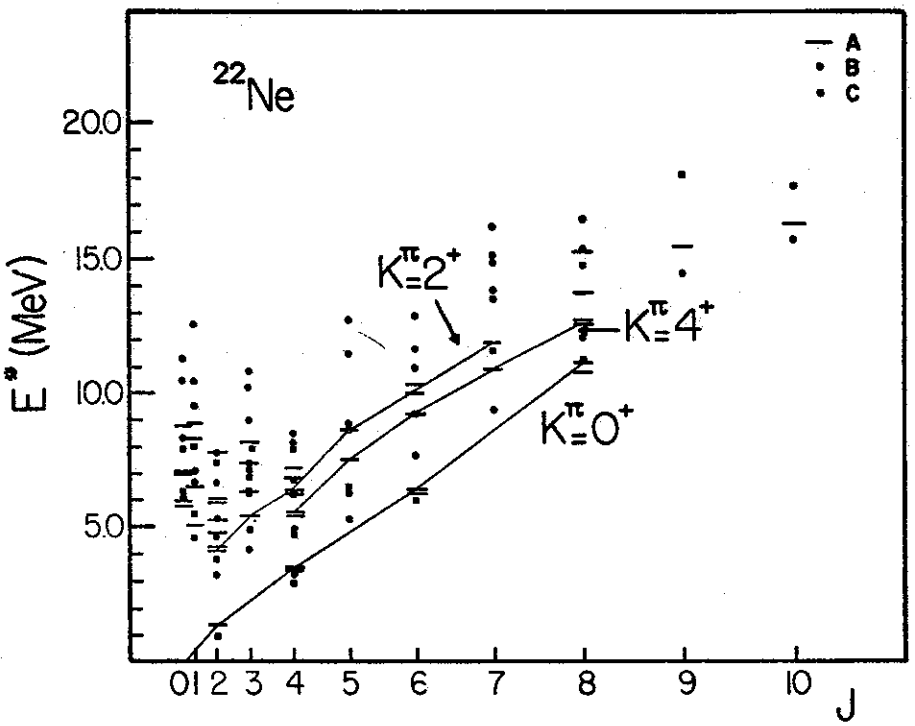

FIGURE 10

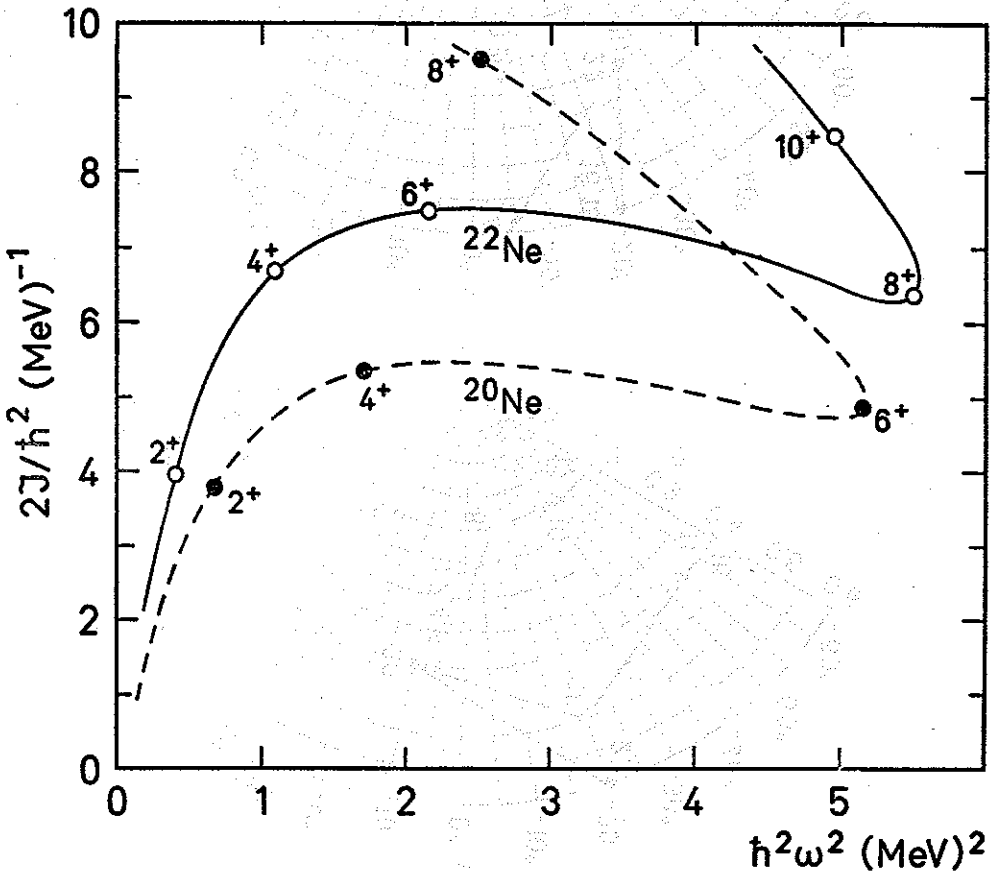

FIGURE 11

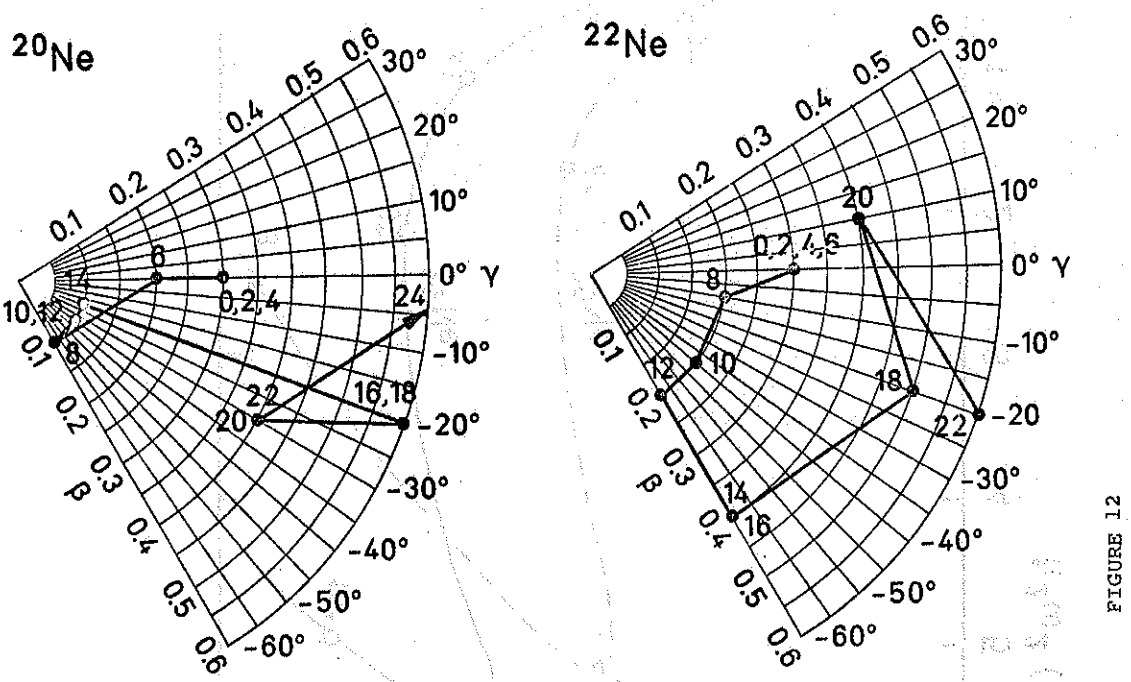
20Ne
22Ne
0.1
0.2
0.3
0.4
0.5
0.6
β
30°
20°
10°
0° γ
-10°
-20°
-30°
-40°
-50°
-60°
0,2,4
6
8
10,12
14
16,18
20
22
24

FIGURE 12